Journal of Undergraduate Chemistry Research, **2020**,19(2), 34

OBSERVATION OF ENHANCED FLUORESCENCE IN VAPOR DEPOSITED FLUORENE ON ALUMINUM OXIDE SUBSTRATE BY ELECTRONIC ENERGY TRANSFER AND SURFACE ROUGHENING

Zackery Moreau*, Katie Nili*, Lexy Gillette*, Jacob Francis*, Bryan Dionisio*, Cassidy Tran*, Christian Kim* and A.M. Nishimura†

Department of Chemistry, Westmont College, Santa Barbara, CA 93108

Abstract

Fluorene was vapor deposited on Al_2O_3 and optically pumped with 250 nm light. A blue fluorescence with λ_{max} ~ 342 nm was observed as the adlayer of fluorene relaxed to the ground state. This fluorescence was found to be dramatically enhanced if an adlayer of *p*-xylene was also vapor deposited as an underlayer to fluorene. Enhancement due to electronic energy transfer occurred as *p*-xylene percolated through the fluorene overlayer. Subsequent to the complete desorption of *p*-xylene, the fluorescence from fluorene remained high by about 10-fold when compared to neat fluorene. This fluorescence enhancement has been postulated to be due to surface modification in the form of surface roughening that can allow significantly greater surface area of the adlayer to be exposed and hence larger number of fluorene molecules that can be excited.

†Corresponding author: nishimu@westmont.edu

Keywords: fluorescence, electronic energy transfer, temperature programmed desorption, TPD, deposition, fluorene, *p*-xylene, 1,4-dimethylcyclohexane, surface roughening

Introduction

Biphenyl and its derivatives are of photophysical interest because of the various dihedral angles that the molecules can have. Due to their high fluorescence quantum efficiency, fluorene, that belong to this class of compounds and its derivatives have had wide interest because of their application to blue LEDs and solar cells.[1-3] Crystal structure of fluorene was first published by Brown and Bortner and others have confirmed that fluorene is planar[4-6] and due to its planarity, fluorene forms excited state dimers or excimers.[7]

Vacuum deposition of aromatic molecules onto cooled surfaces results in amorphous, rather than crystalline multilayers.[8-11] The average intermolecular distance of amorphous adlayers is typically less than the critical distance of 3.0 Å that is necessary to form excimers.[7] If the surface is heated in a temperature programmed desorption (TPD) experiment, the adlayer molecules will undergo a disorder-to-order transition, whereupon the intermolecular distance becomes larger than the critical distance for excimer formation, and molecular fluorescence similar to that observed in solution is observed[7]. Hence, during a TPD experiment, the spectra can serve as a probe to indirectly observe changes in the surface morphology, so that a model of the surface dynamics can be postulated.[8-10]

Previously, we reported that fluorescence from biphenyl was enhanced by the introduction of *p*-xylene due to electronic energy transfer.[12-13] In this paper, attempt is made to differentiate the relative contribution to the fluorescence enhancement by electronic energy transfer from that which occurs because of surface roughening that increases the area and hence the number of fluorophores that can be excited.

Experimental

Fluorene, all three isomers of xylene and *trans*-1,4-dimethylcyclohexane were purchased from commercial sources (Sigma-Aldrich, St. Louis, MO) and their purity was checked by fluorescence. The samples were placed in stainless steel ampoules connected to the ultra high vacuum (UHV) chamber and outgassed by freeze-pump-thaw cycles. Then by means of leak valves, the adsorbates vapors were vacuum deposited from the vapor onto a surface of cryogenically cooled single crystal surface of Al_2O_3 (0001). Diagrammatic details and a camera view of the experimental set-up were given in previous papers[8-10] and are summarized here.

Wavelength-resolved TPD was accomplished using a high pressure Hg arc lamp excitation source in series with a ¼ monochromator that was set at 250 nm. The fluorescence was gathered via a compact diode array spectrometer (Ocean Optics, Dunedin, FL) set at right angle to the excitation source. Experimental hardware integration and control for the TPD, residual gas analyzer, oscilloscope and spectrometer were managed with a system-design software, LabVIEW (Austin, TX). The data acquisition that result from the spectrometer involves a relatively large array of data that exceeds the capacity of spreadsheet software. Thus MATLAB (Natick, MA) was used to generate the wavelength-resolved TPD figures presented in this article.

For the TPD experiment, the temperature was linearly ramped at 2 K/s. A chromel-alumel thermocouple that was in thermal contact with the Al_2O_3 alumina crystal surface sent a voltage to an analog-to-digital converter that in turn was connected to a computer that controlled a power supply. This power supply fed current through a tantalum foil that was in thermal contact with the alumina, and resistively heated the Al_2O_3. The crystal temperature was continuously monitored while sufficient current was sent to the tantalum foil to keep heating the crystal. A PID (proportional integral derivative) control subroutine module in the LabVIEW program was used to insure a constant temperature ramp rate.

The adlayer coverages were determined by using a diode laser that was directed at the surface during deposition.[11] The integrated mass spectral peaks were calibrated against the resulting optical interference experiment and the coverages (Θ) are report-

ed in monolayers (ML) with an error of ± 30% . The activation energy for desorption, E_a, was calculated by Redhead analysis by assuming a first-order desorption kinetics as described by King. It is based on the mass spectral peak desorption temperature, T_p [13-15]. The uncertainties in the desorption temperatures and the propagated error in the activation energies are ± 1%.

In order to distinguish electronic energy transfer and surface roughening, an annealing experiment was performed. A layer of *p*-xylene was deposited on the cold alumina crystal followed by the deposition of a fluorene layer. Subsequent to vapor deposition, the temperature of the adlayer was ramped at the same 2K/s to a predetermined annealing temperature of 210 K and held at that temperature within ± 1 K for 20 s. At this annealing temperature, the underlayer of *p*-xylene was determined with the residual gas analyzer to have completely desorbed. The substrate was allowed to cryogenically cool down to 135 K and then a TPD experiment performed. In the post-annealing TPD experiment, the residual gas analyzer data showed only fluorene and no additional *p*-xylene was desorbed.

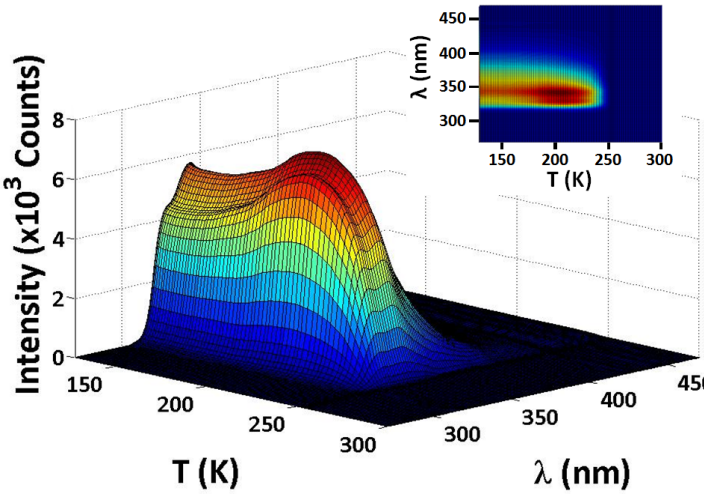

Figure 1. Wavelength resolved TPD of neat fluorene. $\Theta_{fluorene}$ ~ 24 ML. Inset: wavelength as a function of temperature

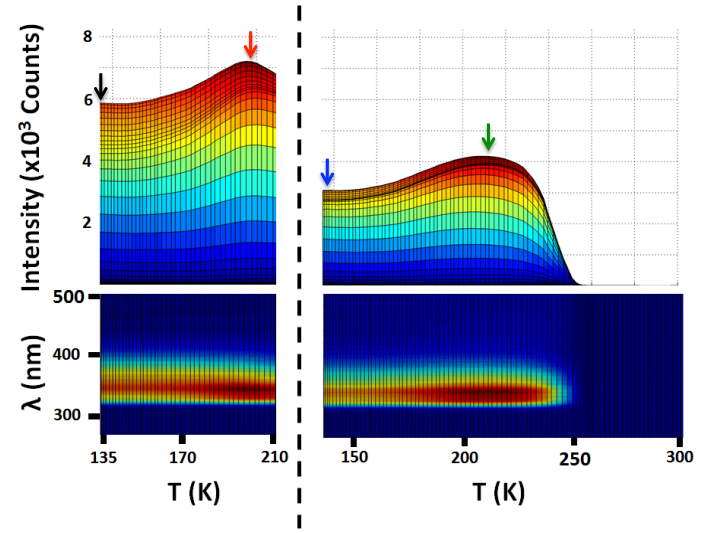

Figure 2. Annealing plots of neat fluorene. $\Theta_{fluorene}$ ~ 24 ML. During the anneal on the left and after the anneal on the right. Arrows indicate locations on the TPD that were noted in the text.

Results and Discussion

Neat fluorene:

The wavelength resolved TPD of fluorene is shown in Figure 1. T_p is 244 K with E_a ~ 63.4 kJ/mol. The main feature was that the emission from the excimeric amorphous fluorene with a λ_{max}~342 nm increased in intensity until a maximum was reached at about 200 K. An accompanying shoulder that was blue shifted by about 5 nm also increased in intensity with a maximum at about 200 K, the disorder-to-order transition.

Shown in Figure 2 are the results of the annealing experiment as explained in the experimental section above. The top left plot shows the fluorescence intensity as a function of temperature and the bottom left shows the corresponding wavelength spectrum versus temperature. Both the top left and bottom left plots share the same temperature axis. Plots stop at the annealing temperature of 210 K when annealing was allowed to occur for 20 s. In the TPD experiment of the annealed fluorene, the fluorescence intensity as a function of temperature is plotted on the top right quadrant. The lower plot on the right shows the corresponding wavelength versus temperature plot. The bottom left spectrum shows the aforementioned small but distinct blue shift at about 200K which is where the disorder-to-order transition. On the bottom right, the blue-shifted spectrum persists through the entire TPD. The conclusion is that once the adlayer underwent the disorder-to-order transition, the ordered form of the fluorene persisted because it was thermally more stable. The intensity plot of the annealed fluorene shows that the blue-shifted species remained but at half the intensity at the beginning of the TPD (blue arrow, top right) compared to the unannealed fluorene (black arrow, top left). The maximum intensity of the annealed fluorene at 200 K (green arrow, top right) is about 60% of the maximum intensity of the unannealed fluorene (red arrow, top left).

It should be noted that the intensity of the fluorescence of fluorene increased with temperature up to 200 K. Since this maximum was observed in neat fluorene and in bilayers (see below), this is

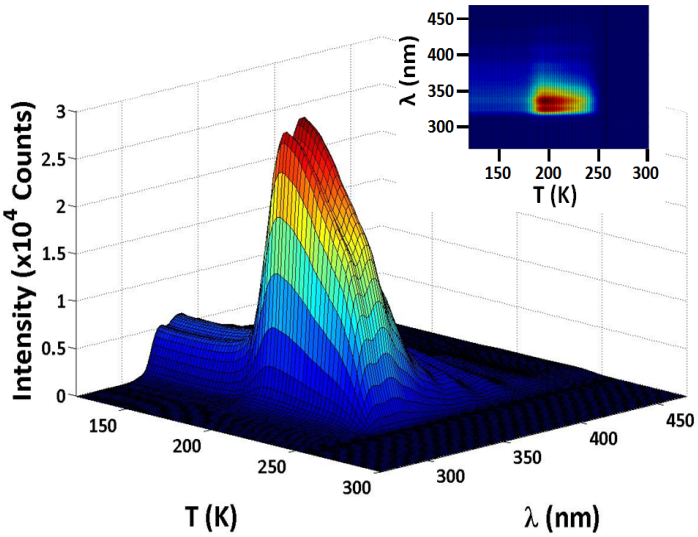

Figure 3. Wavelength resolved TPD of *p*-xylene/fluorene bilayer. $\Theta_{p\text{-xylene}}$ ~ 103 ML and $\Theta_{fluorene}$ ~ 20 ML. Inset: top view (wavelength as a function of temperature).

an intrinsic molecular property. Since this property was thermally reversible and independent of cycling of the surface temperature, a relaxation route must be present in solid fluorene that is Arrhenius in form. One possibility is that at 200 K, CH vibration mode might be coupling to the electronic state responsible for the radiative relaxation process.

p-xylene/fluorene bilayer:

Figure 3 shows the effect of the *p*-xylene underlayer upon the fluorene. T_p of p-xylene is 179 K and E_a is 46 kJ/mol. As expected, the fluorescence intensity increased as the adlayer temperature reached the desorption temperature of *p*-xylene (179 K) and *p*-xylene began to percolate through the upper layer of fluorene.

Similar to the placements of the plots in Figure 2, Figure 4 shows fluorescence intensity of the *p*-xylene/fluorene bilayer prior to and after the anneal. What is immediately apparent is the almost 6 fold increase in the fluorescence intensity (red arrow, top left) at 200 K compared to the initial intensity (black arrow). Subsequent to annealing the fluorene adlayer and after all of the *p*-xylene had desorbed, the initial fluorescence intensity of fluorene (blue arrow, top right) was almost 3-fold higher than prior to the anneal (black arrow top left). Since *p*-xylene has completely desorbed and little to none of the fluorene has been lost, this increase in intensity must be due to the surface roughening that resulted during the passage of *p*-xylene through the fluorene adlayer.

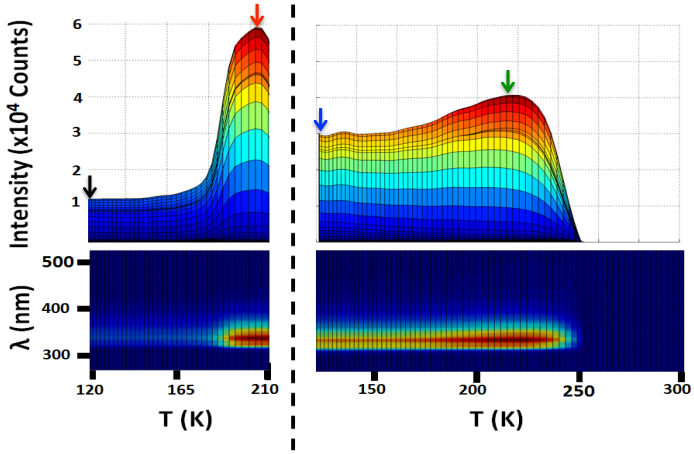

Figure 4. Annealing plots of *p*-xylene/fluorene bilayer. $\Theta_{p\text{-xylene}}$ ~ 106 ML and $\Theta_{fluorene}$ ~ 26 ML. During the anneal on the left and after the anneal on the right. Arrows indicate locations on the TPD that were noted in the text..

In order to determine the optimum coverage ratio of *p*-xylene to fluorene responsible for the fluorescence enhancement shown in Figure 3 and the left half of Figure 4, a plot was prepared. Figure 5 shows the intensity of fluorene fluorescence at 200 K as a function of *p*-xylene to fluorene coverage ratio. More specifically, the plot shows the ratio of the maximum intensity of the fluorescence at 200 K (red arrow in Figure 4) to the initial intensity (black arrow

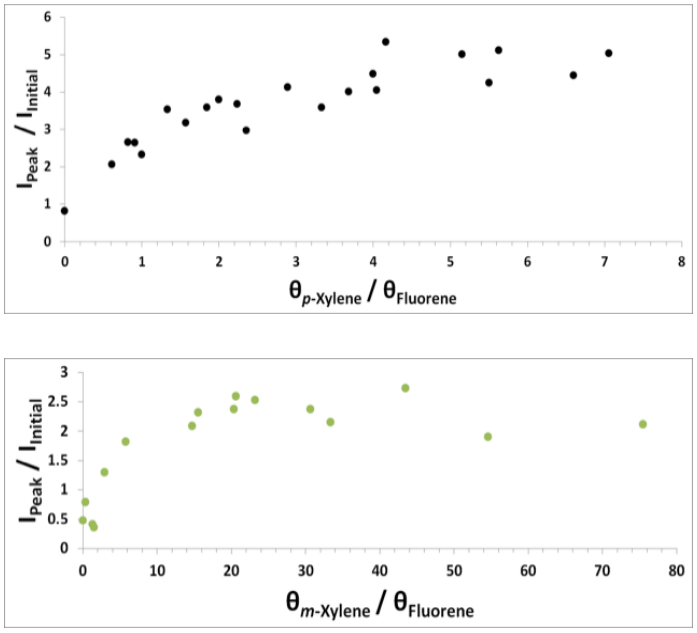

Figure 5. *Top*: bilayers of *p*-xylene/fluorene, $I_{peak}/I_{initial}$, ratio of the peak intensity (red arrow, Fig. 4) to the initial intensity (black arrow, Fig. 4) as a function of the relative coverages of *p*-xylene to fluorene, $\Theta_{p\text{-xylene}}$ (ML)/$\Theta_{fluorene}$ (ML). *Bottom:* bilayers of *m*-xylene/fluorene, $I_{peak}/I_{initial}$, ratio of the peak intensity to the initial intensity as a function of the relative coverages of *m*-xylene to fluorene, $\Theta_{m\text{-xylene}}$ (ML)/$\Theta_{fluorene}$ (ML).

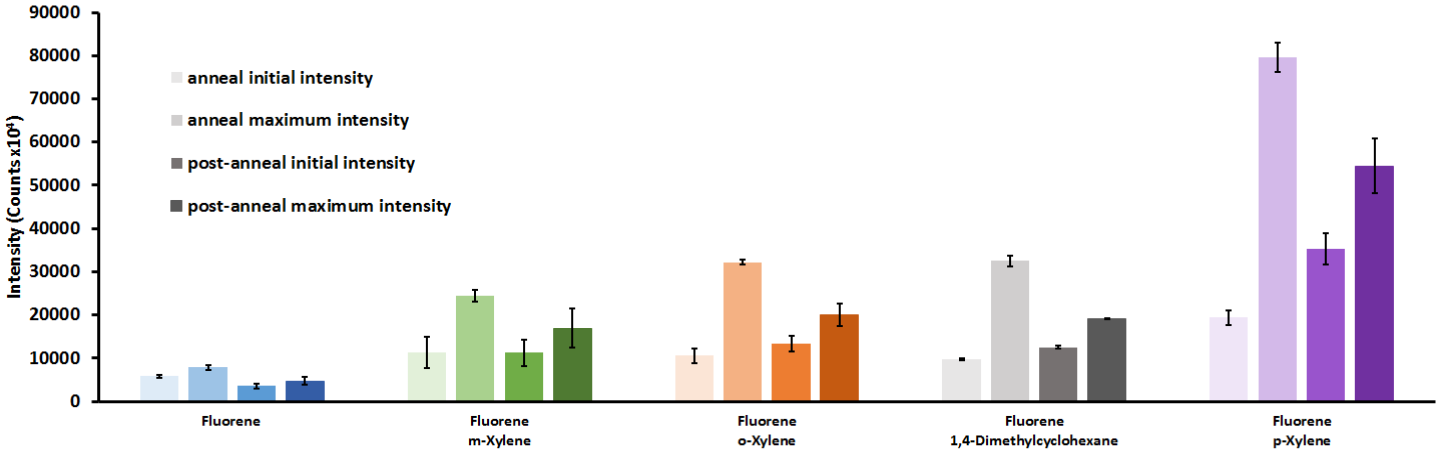

Figure 6. Summary of data for neat fluorene and bilayers of *m*-xylene, *o*-xylene, 1,4-dimethylcyclohexane, *p*-xylene with fluorene. *1st bar* = initial TPD intensity *prior* to anneal (black arrows in Figs. 2 and 4), *2nd bar* = maximum intensity prior to anneal (red arrows in Figs. 2 and 4), *3rd bar* = initial TPD intensity after anneal (blue arrows in Figs. 2 and 4) and *4th bar* = maximum intensity after anneal (green arrows in Figs. 2 and 4).

in Figure 4) or $I_{peak}/I_{initial}$ as a function of the coverage ratio: $\Theta_{p\text{-xylene}}$ (ML)/$\Theta_{fluorene}$ (ML). The leveling of the plot occurred where the intensity ratio of about 5 intersects the coverage ratio of $\sim 5 \pm 2$. In Figure 3 and 4, the coverage ratios ($\Theta_{p\text{-xylene}}$(ML)/$\Theta_{fluorene}$ (ML)) were 5.2 and 4.1, respectively and therefore, just about where the relative intensity $I_{peak}/I_{initial}$ has leveled.

The fluorescence enhancement that is shown in Figure 3 and the left side of Figure 4 was due to a combination of electronic energy transfer and surface roughening. In order to determine the relative contribution of each, benchmark measurements were made of the following: a) initial intensity (black arrow in Figure 4) since this is related to the number of amorphously prepared fluorene molecules that were present in the adlayer, b) the peak intensity prior to the anneal (red arrow in Figure 4) since this is due to fluorescence from both resonance energy transfer from *p*-xylene donor to fluorene acceptor and increased fluorescence due to the surface roughening, c) the initial fluorescence intensity after the anneal (blue arrow Fig. 4) since this is due to the surface roughened bilayer and d) the intensity maximum after the anneal (green arrow, Fig. 4). The effect of surface roughening is the difference between the initial intensity after the anneal for the bilayer system (blue arrow in Figure 4) and the corresponding intensity of the neat annealed fluorene (blue arrow in Fig. 2). The peak intensity that is observed during the TPD experiment after the anneal (green arrow in Fig. 4) is due to the surface roughened *and* the intensity that is observed without the surface roughening (green arrow in Fig. 2). This gives another point of reference for the *p*-xylene's effect on surface roughening. Since the coverages of fluorene were approximately the same for both Figures 2 and 4, the order of magnitude higher intensities at both benchmark points (green and blue arrows) were the degrees to which surface roughening enhanced the fluorescence.

Similar experiments were performed on *m*-xylene. For *m*-xylene the leveling of the $I_{peak}/I_{initial}$ occurred at a higher $\Theta_{m\text{-xylene}}$ (ML)/$\Theta_{fluorene}$ (ML) coverage ratio, as shown in the lower plot in Figure 5. In that system, leveling occurred when the coverage ratio was $\sim 20 \pm 2$. Although not shown here, similar experiments were also done with *o*-xylene. A comparative histograms plot of the 4 benchmark measurements can be seen in Figure 6. The plot summarize the results for neat fluorene, and bilayers of *p*-, *m*- and *o*-xylene with

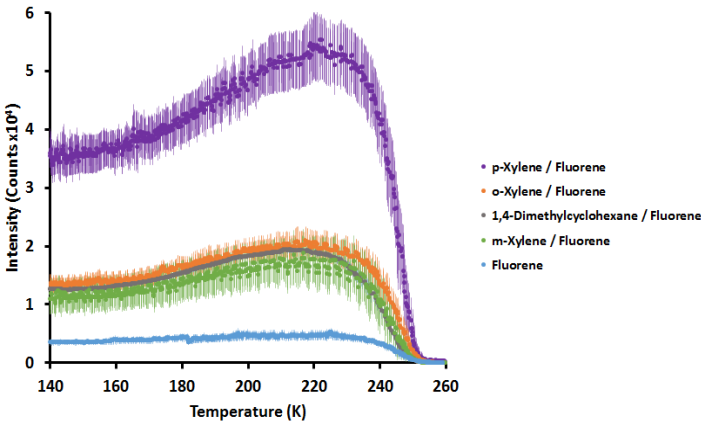

Figure 7. Intensity of the blue-shifted fluorene fluorescence after the anneal for neat fluorene in blue, bilayers of *trans*-1,4-dimethylcyclohexane/fluorene in dark green, *m*-xylene/fluorene in light green, *o*-xylene/fluorene in orange, and *p*-xylene/fluorene in purple.

fluorene are shown in Figure 6 as histograms of the 4 benchmark measurements. From Figures 2 and 4, the intensity shown with black arrows is the first bar of each set, the intensity shown with red arrow is the next bar on the histogram, the intensity in blue is the next bar and finally, intensity in green is shown. Comparison of the 3rd histogram bars give the effect of surface roughening and these were 3-fold and 4-fold increases for bilayers with *m*-xylene and *o*-xylene, respectively. In addition, the initial intensity after the anneal (third histogram bar in each bilayer set in Figure 6) are higher than prior to the anneal (first histogram bar). This is due to the irreversibility and thermal stability of the roughened surface.

Since a saturated hydrocarbon is not electronically excited by the 250 nm excitation source, *trans*-1,4-dimethylcyclohexane was used as an underlayer to fluorene in order to factor out the effect due to electronic energy transfer. The fluorescence intensity as a function of temperature during the TPD after annealing all of the bilayers along with neat fluorene are shown in Figure 7. As can be seen from Figures 6 and 7, the effect of *trans*-1,4-dimethylcyclohexane was very similar to *o*- and *m*-xylene within experimental error. This means that electronic energy transfer was absent in the TPD of *o*- and *m*-xylene/fluorene bilayer and the enhancement in the fluorene fluorescence in those bilayer systems must be due solely to surface roughening.

As asserted previously, during the TPD experiment, the enhancement in fluorescence that was observed for the *p*-xylene/fluorene bilayer system was due to both electronic energy transfer *and* surface roughening. To determine the contribution of electronic energy transfer alone, the fluorescence intensity after annealing must be subtracted from the fluorescence before annealing, but at the same temperature at which percolation of the *p*-xylene occurred. This meant that the intensity indicated by the green arrow in Figure 4 must be subtracted from the intensity shown by the red arrow. This difference is about 50% of the intensity shown with green arrow. In other words, about 33% (50/150) of the intensity indicated by the red arrow is due to electronic energy transfer, less than 10% is due to fluorescence from fluorene itself and the rest (~57%) is due to surface roughening.

If a comparison is made of the initial intensities after the anneal which is shown on the 3rd bars for the sets of bilayers in Figure 6, the efficiency of *p*-xylene to roughen the surface is about 3-fold greater than for the other underlayers which at first, seems excessively high considering the structural similarities of the underlayers. Perhaps the molecular and electronic similarities of *p*-xylene to fluorene might explain the degree to which *p*-xylene disrupts the ordered form of fluorene, but this idea needs further investigation.

Finally, it should be noted that the initial intensities of the bilayers are significantly higher than in the neat fluorene (first bar of the 5 sets of histograms in Figure 6) even though, presumably the two layers were prepared distinct and intact. This could be due to roughening at the interface between the two layers. Although not shown here, a plot of the initial intensity as a function of *p*-xylene to fluorene coverage showed an almost immediate (at ratios of coverage of *p*-xylene to fluorene less than 1) increase in intensity to the level of the bilayer shown in Figure 4 with the black arrow. Another evidence that supported this explanation was that the increase in the difference (i.e. slopes) between the intensities of the

bilayer compared to that for the neat fluorene during the TPD experiment increased with temperature (See Figure 7). As the lower layer mixed into the upper layer, this interface increased in volume.

References:

1). Grimsdale. A.C. and Jacob, J., Polymer-Based LEDs and Solar Cells in *Reference Module in Materials Science and Materials Engineering* **2016,** Elsevier.
2). Tirion, D., Romain, M., Rault-Bethelot, J. and Poriel, C., *J. Materials Chem*., **2012**, *22*, 7149-7157.
3). Kim, Y.H., Shin, D.C., You H., and Soon, S.K., *Polymer*, **2005**, *46*, 7969-7973.
4). Brown, G.M. and Bortner, M.H., *Acta Crystallographica*, **1954**, *7*, 139.
5). Gerkin, R.E., Lundstedt, A.P., Reppart, W.J., *Acta Crystallographica*, *Section C: Crystal Structure Communications*, **1984**, *C40*, 1892-2894.
6). Bel'skii, V.K., Zavodnik, V.E. and Vozzhennikov, V.M., *Acta Crysallographica, Section C: Crystal Structure Communication*, **1984**, *C40*, 1210-1211.
7). Birks, J.B. *Photophysics of Aromatic Molecules*, Wiley-Interscience, London, (1970) pp. 301-769.
8). Lau, S., Ryan, H.E., Baer, B.B., Martin, K.A. and Nishimura, A.M. *JUCR,* **2012**, *11*, 107-111.
9). Ryan, H.E., Lau, S., Baer, B.B., Martin K.A. and Nishimura, A.M. *JUCR*, **2012**, *11*, 90-93.
10). Gardner, S.R., Selby, L.M., Teranishi, R.K., Douglas, M.S., Simonds, S.W., Martin, K.A. and Nishimura, A.M. *J. Lumin*., **2013**, *134*, 657-664.
11). Fonda, B.D., Condie, M.K., Moreau, Z.E., Shih, Z.I., Dionisio, B. Fitts, A., Foltz, L., Nili, K. and Nishimura, A.M., *J. Phys. Chem. C*, **2019**, *123*, 26185-26190.
12). Condie, M.K., Moreau, Z.E. and Nishimura, A.M., JUCR, 2019, 18, 15-18.
13). Redhead, P.A. *Vacuum*, **1962**, *12*, 203-211.
14). Lord F.M. and Kittelberger, J.S.. *Surf. Sci.*, **1974**, *43*, 173-182.
15). King, D.A.. *Surf. Sci*., **1975**, *47*, 384-402.